

ARTICLE

Received 26 Feb 2017 | Accepted 12 May 2017 | Published 29 Jun 2017

DOI: 10.1038/ncomms15929

OPEN

Jahn-Teller distortion driven magnetic polarons in magnetite

H.Y. Huang^{1,2}, Z.Y. Chen³, R.-P. Wang⁴, F.M.F. de Groot⁴, W.B. Wu¹, J. Okamoto¹, A. Chainani¹, A. Singh¹, Z.-Y. Li⁵, J.-S. Zhou⁵, H.-T. Jeng³, G.Y. Guo^{6,7}, Je-Geun Park^{8,9}, L.H. Tjeng¹⁰, C.T. Chen¹ & D.J. Huang^{1,3}

The first known magnetic mineral, magnetite, has unusual properties, which have fascinated mankind for centuries; it undergoes the Verwey transition around 120 K with an abrupt change in structure and electrical conductivity. The mechanism of the Verwey transition, however, remains contentious. Here we use resonant inelastic X-ray scattering over a wide temperature range across the Verwey transition to identify and separate out the magnetic excitations derived from nominal Fe^{2+} and Fe^{3+} states. Comparison of the experimental results with crystal-field multiplet calculations shows that the spin-orbital dd excitons of the Fe^{2+} sites arise from a tetragonal Jahn-Teller active polaronic distortion of the Fe^{2+}O_6 octahedra. These low-energy excitations, which get weakened for temperatures above 350 K but persist at least up to 550 K, are distinct from optical excitations and are best explained as magnetic polarons.

¹National Synchrotron Radiation Research Center, Hsinchu 30076, Taiwan. ²Program of Science and Technology of Synchrotron Light Source, National Tsing Hua University, Hsinchu 30013, Taiwan. ³Department of Physics, National Tsing Hua University, Hsinchu 30013, Taiwan. ⁴Inorganic Chemistry and Catalysis, Utrecht University, Universiteitsweg 99, 3584 CG Utrecht, The Netherlands. ⁵Department of Mechanical Engineering, Texas Material Institute, University of Texas at Austin, Austin, Texas 78712, USA. ⁶Department of Physics, National Taiwan University, Taipei 10617, Taiwan. ⁷Division of Physics, National Center for Theoretical Sciences, Hsinchu 30013, Taiwan. ⁸Department of Physics and Astronomy, Seoul National University, Seoul 08826, Korea. ⁹Center for Correlated Electron Systems, Institute for Basic Science, Seoul 08826, Korea. ¹⁰Max Planck Institute for Chemical Physics of Solids, Nöthnitzerstr. 40, 01187 Dresden, Germany. Correspondence and requests for materials should be addressed to D.J.H. (email: djhuang@nsrrc.org.tw).

Since its first X-ray structural elucidation by Bragg¹ a hundred years ago and the discovery of the Verwey transition^{2,3}, magnetite (Fe_3O_4), has received much attention for decades. Even today, it attracts significant scientific and technological interest for its applications in ultrafast magnetic sensors⁴, palaeomagnetism⁵, nanomedicine carriers⁶, and so on. Fe_3O_4 becomes ferrimagnetic below $T_c \sim 850$ K, followed by an abrupt decrease in its electrical conductivity by two orders of magnitude as the temperature is cooled below T_V . In this first known magnet to mankind, one-third of Fe sites, termed *A*-sites, are tetrahedrally (T_d) coordinated with oxygens; the other two-thirds, termed *B*-sites, have octahedral (O_h) coordination. Verwey first suggested a Fe^{2+} – Fe^{3+} charge-ordering occurring on the *B*-sites as the driving force of this transition. There are two major schools of interpretation: the first one interprets the Verwey transition as a transition driven by charge/orbital ordering^{7–17}. The second one exploits the mechanism of a lattice distortion-driven electron–phonon coupling^{18–22} enhanced by the on-site Coulomb interaction and thus opens a gap at the Fermi energy when the temperature is lowered below the Verwey transition temperature T_V .

Although numerous investigations have been carried out to verify the charge localization on the *B*-sites, the charge-ordering pattern of magnetite is subtle and still elusive^{19,20}. While it is agreed that the charge disproportionation involves changes in the nominal Fe^{2+} and Fe^{3+} states associated with the *B*-sites, X-ray diffraction studies of the low-temperature phase of magnetite microcrystals^{15,17} revealed that the t_{2g} electrons of the *B*-sites are not fully localized in the form of Fe^{2+} states. Instead, the electrons are distributed over linear three-Fe-site units termed trimers, which are coupled to the T_d Jahn-Teller distortion of *B*-site Fe^{2+}O_6 octahedra, as illustrated in Fig. 1. To the first approximation, the *B*-site Fe^{3+}O_6 octahedra are Jahn-Teller-inactive. The tetragonal distortion of *B*-site Fe^{2+}O_6 octahedra removes the degeneracy of t_{2g} orbitals, in going from O_h symmetry to D_{4h} symmetry. In the absence of spin-orbit coupling, an effective energy separation $\Delta_{t_{2g}}$ between d_{xy} and d_{yz}/d_{zx} is created if the four Fe–O bonds in the *xy* plane are elongated or contracted. The trimeron scenario then indicates that the Verwey transition is essentially due to an ordering of trimers. Because previous results of optical conductivity²³ and photoemission^{24–27} showed the pseudogap feature of magnetite above T_V , and results of entropy analysis²⁸, neutron/X-ray diffuse scattering²⁹ and anomalous phonon broadening²² revealed the short-range order above T_V , one important open question is whether trimeron correlations persist in the cubic phase at temperatures above T_V . Combining these short-range correlations of polaronic characters with the spin degrees of freedom of t_{2g} electrons, one can expect magnetic polarons in magnetite.

Here we present measurements of resonant inelastic X-ray scattering (RIXS)^{30,31} at the Fe L_3 -edge on magnetite to reveal the low-energy spin–orbital excitations of Fe^{2+} ions in both the monoclinic and cubic phases. To the best of our knowledge, the magnetic excitations derived from the local tetragonal distortion field of Fe^{2+} ions, that is, magnetic polarons, have not been reported to date. In combination with crystal-field multiplet calculations, we show the existence of magnetic polarons in magnetite which is driven by the Jahn-Teller distortion.

Results

Fe L_3 -edge RIXS. Figure 2a shows the Fe L -edge X-ray absorption spectrum of magnetite. By comparing with crystal-field multiplet calculations (see Supplementary Fig. 1), it is understood that the absorption-energy centroid of Fe^{2+} ions is lower than that of

Fe^{3+} ions by ~ 1 – 2 eV, consistent with earlier work^{32–34}. Accordingly, the features at X-ray energies of 706.0 and 707.5 eV originate from the absorption of octahedrally coordinated *B*-site Fe^{2+} states, while the maximum intensity feature at 708.8 eV is dominated by absorption from the Fe^{3+} ions of both the *B*-site octahedral and *A*-site tetrahedral symmetries.

The colour map of RIXS intensity measured at 80 K in the plane of incident photon energy versus energy loss shown in Fig. 2b presents the evolution of the RIXS spectral profile associated with Fe^{2+} and Fe^{3+} ions as detailed in the following. When the incident X-ray energy was set to below 707.5 eV, we observed *dd* excitations of Fe^{2+} with energy losses at 2.8 ± 0.05 , 1.65 ± 0.05 and 1.16 ± 0.05 eV shown in Fig. 2c, and also a broad excitation centred at 200 meV shown in Fig. 2d. If the incident X-ray energy goes beyond 707.5 eV, the 1.16-eV *dd* excitation of Fe^{2+} begins to evolve into a fluorescence that has a constant X-ray emission energy independent of incident energy. With the incident X-ray energy set to 708.8 eV, RIXS excitations arise mostly from Fe^{3+} ions of octahedral or tetrahedral symmetry.

Figure 2d shows two RIXS features centred at 90 and 200 meV in a magnified plot of energy loss below 0.7 eV. Measurements carried out by varying the scattering angle suggested that these two low-energy excitations do not disperse in momentum space (see Supplementary Fig. 2). The 200-meV excitation has a full-width at half-maximum larger than the instrumental energy resolution. This broad RIXS feature resonates near the L_3 -edge of Fe^{2+} and almost disappears for incident energy above 708 eV, at which the other excitation centred at 90 meV emerges. The 90-meV excitation has a full-width at half-maximum nearly equal to the instrumental energy resolution and resonates at 708.4 eV. The distinct incident X-ray energies for these resonant excitations indicate that the 200- and 90-meV features arise from Fe^{2+} and Fe^{3+} states, respectively.

Many experimental^{35–37} and theoretical^{30,38–41} studies have shown that L -edge RIXS allows spin–flip processes that are not accessible with optical spectroscopy²³. For example, if both the incident and scattered X-rays are π -polarized, the spin–flip excitation of d_{yz} is allowed owing to the spin–orbit coupling in the $2p$ core state. In the present RIXS measurements with a 90° -scattering geometry (see Supplementary Fig. 2a), the intensity of elastic excitation with incident X-rays of π polarization is reduced in comparison with that of σ polarization, and spin–flip excitations are effectively revealed. In addition, the cross-section

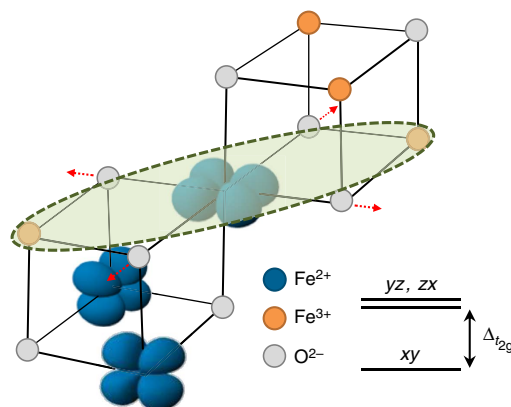


Figure 1 | Trimeron scenario and t_{2g} energy-level splitting. Illustration of the orbital ordering of *B*-site Fe^{2+} in Fe_3O_4 and the corresponding t_{2g} energy-level splitting for a Fe^{2+} ion in a negative $\Delta_{t_{2g}}$ crystal field. A trimeron is indicated with a dashed oval. The elongation of the four Fe–O bonds in the *xy* plane are indicated with arrows.

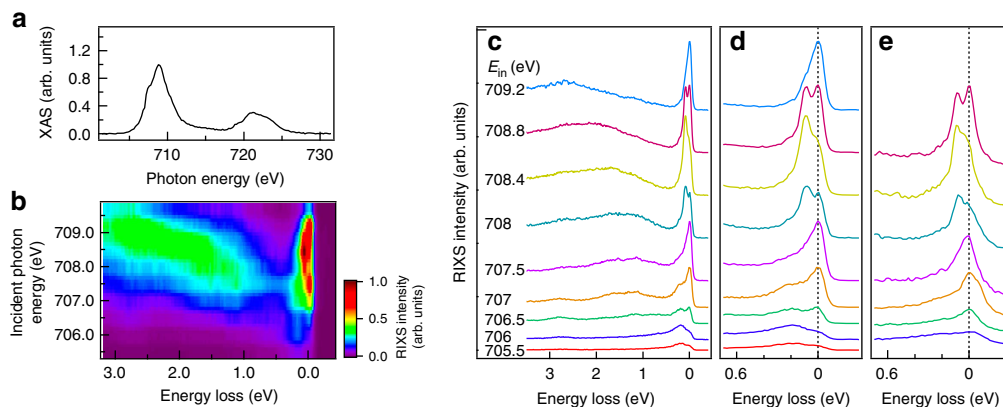


Figure 2 | RIXS measurements of Fe_3O_4 . (a) Fe L -edge X-ray absorption spectrum (XAS) spectrum measured in the fluorescence yield mode through the summation of all inelastic X-ray intensities taken at room temperature $T = 300$ K. The XAS is plotted with correction for self-absorption. The incident X-ray energy resolution was 0.5 eV. (b) Colour map of RIXS intensity after correction for self-absorption in the plane of incident photon energy versus energy loss recorded at $T = 80$ K. (c–e) RIXS spectra plotted in terms of energy loss with a vertical offset for clarity. They were recorded by using π -polarized incident X-rays under the scattering geometry of the scattering angle $\phi = 90^\circ$ and the incident angle $\theta = 20^\circ$. Panels c,d were measured at 80 K and e was measured at 550 K.

of L_3 -edge RIXS for a magnetic excitation is usually larger than that for a phonon excitation³⁵. Because O K -edge RIXS-probe excitations derived from bimagnons⁴² and phonons⁴³, we performed O K -edge RIXS measurements to probe the phonons of Fe_3O_4 . Our data shown in Supplementary Fig. 4 reveal an excitation at 70 meV in the O K -edge RIXS, indicating that the observed 90-meV feature of the Fe L_3 -edge RIXS has a small contribution from phonon excitation^{44,45}.

Multiplet RIXS calculations. In order to characterize the origin of the observed excitations, we undertook crystal-field multiplet calculations for the B -site Fe^{3+} and Fe^{2+} ionic configurations. See the Methods section, Supplementary Note 2 and Supplementary Figs 5 and 6 for calculation details.

Multiplet calculations carried out for the B -site Fe^{3+} ions under an exchange molecular field of 90 meV, as shown in Supplementary Fig. 5d, explain the observed excitation energy of 90 meV well. This is consistent with the 100-meV Zeeman splitting induced by the molecular field deduced from the Curie temperature of magnetite and the exchange coupling constants⁴⁶. This spin-flip energy also agrees with the energy of the nearly dispersionless mode at 80–85 meV observed in inelastic neutron scattering^{46,47}. For an individual Fe^{3+} site, the intensity of the 90-meV RIXS feature can change under a spin reorientation as magnetic RIXS is sensitive to the spin direction with respect to the incident polarization. However, RIXS measurements of B -sites Fe^{3+} reflect an average of eight non-equivalent Fe^{3+} . Each of these non-equivalent Fe^{3+} B -sites can make different contributions to the intensity of the 90-meV feature, and our measured RIXS spectra suggest that these changes are beyond our experimental sensitivity. Although we cannot totally rule out phonon contributions, the 90-meV L_3 -edge RIXS excitation is best explained as a result of spin-flip excitations of Fe^{3+} ions, like magnetic excitations observed in the RIXS of Fe pnictide superconductors³⁶, cuprates^{30,37,40} and nickelates^{38,41}.

The ground state of the octahedral Fe^{2+} ion is a high-spin ${}^5T_{2g}$ state with $S = 2$. According to Hund's rule, out of the six $3d$ electrons of the Fe^{2+} ion, five $3d$ electrons occupy spin-up states $t_{2g}^{\uparrow} e_g^{\uparrow}$; the remaining one electron occupies one of the three spin-down orbitals t_{2g}^{\downarrow} . When the spin-orbit effect of $3d$ electrons couple a pseudo-orbital angular momentum $\tilde{L} = 1$ to $S = 2$, the ${}^5T_{2g}$ state splits into three manifolds of pseudo-angular momenta

$\tilde{J} = 1, 2$ and 3. That is, there are effectively 15 separate states from Fe^{2+} , as the ${}^5T_{2g}$ ground state is split by the combination of these interactions. For the broad 200-meV RIXS feature associated with the octahedral Fe^{2+} states, the excitation energy is too large to be explained in terms of spin-flip excitations only. We carefully checked the effect of the local Jahn-Teller distortion to explain the energy of the observed excitations to understand the nature of this feature. From an extensive set of RIXS calculations of Fe^{2+} with varied tetragonal distortions as shown in Supplementary Fig. 6, we found that the average RIXS spectrum calculated using $H_{\text{ex}} = 90$ meV and $\Delta_{t_{2g}} = -22, -26$ and -30 meV explains the measured spectrum most satisfactorily, as demonstrated in Supplementary Fig. 5f. Figure 3a shows the calculated low-energy RIXS excitations of Fe^{2+} in the form of incident photon energy versus energy-loss maps. The calculated RIXS obtained by including the tetragonal distortion, exchange interaction and $3d$ spin-orbit coupling matches fairly well with the experimental data.

Discussion

In comparison with the magnified intensity map of RIXS measurements shown in Fig. 3b, calculations using a molecular field $H_{\text{ex}} = 90$ meV and $\Delta_{t_{2g}} = -26 \pm 4$ meV reproduce the energy-loss features suitably. For the 200-meV excitation, the experimental resonance starts at an energy lower than that of the resonant quasi-elastic scattering of Fe^{2+} and its energy range is broad, while the calculated resonance starts at a higher energy with a narrow range. This discrepancy is attributed to differences in the dynamics of $3d$ orbitals due to core-hole effects in intermediate states. These effects do not affect the energy loss of excitation spectra because the core holes are filled in the RIXS final state. As is typical of RIXS calculations reported in the literature, our calculations do not include such core-hole effects, and hence do not reproduce the incident energy dependence perfectly, but our calculations correctly reproduce the energy-loss features.

Figure 3c presents calculated RIXS spectrum in comparison with measurements of the incident X-ray energy set to 707 eV, at which the 200-meV RIXS feature is most pronounced. The negative value of $\Delta_{t_{2g}}$ signifies that the energy of d_{xy} is lower than that of d_{yz}/d_{zx} , that is, tetragonally distorted Fe^{2+}O_6 octahedra with elongated Fe–O bonds in the xy plane. This shows that the tetragonal distortion is directly related to a polaronic distortion of

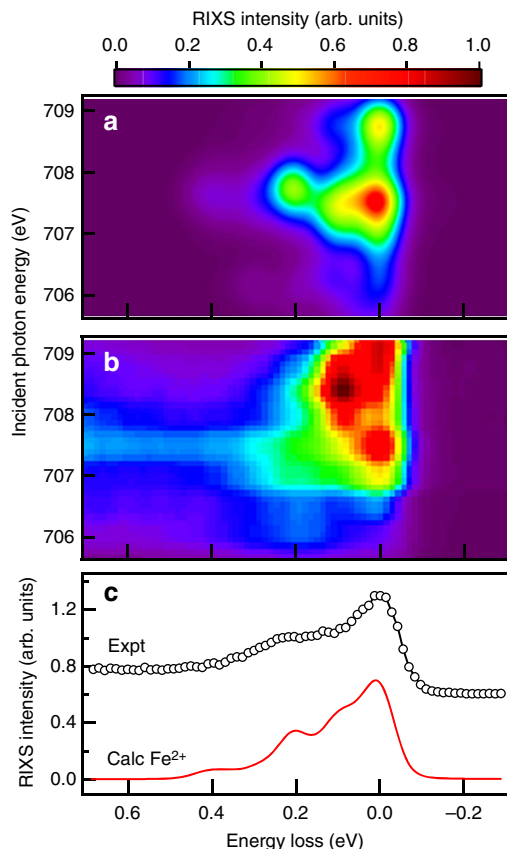


Figure 3 | Calculated RIXS of Fe^{2+} in comparison with measurements.

(a) Calculated RIXS intensity map of B -site Fe^{2+} by using $H_{\text{ex}} = 90$ meV, $\Delta_{t_{2g}} = -26 \pm 4$ meV and the $3d$ spin-orbit coupling $\zeta_{3d} = 52$ meV. The resonance photon energy of Fe^{2+} is set to the experimental resonance energy 707.5 eV. The core-hole lifetime width is set to 200 meV, and the final-state lifetime width is set to 10 meV. This calculated intensity map presents the average RIXS intensity for the magnetic easy axis along the [100], [010] and [001] directions, and are plotted after Gaussian broadening of width 500 and 80 meV for the incident photon energy and the energy loss, respectively. (b) A magnified intensity map of RIXS measurements of single-crystal Fe_3O_4 extracted from Fig. 2b. (c) Comparison of measured (expt) and calculated (calc) RIXS spectra. Open circles are measurements with incident X-rays of 707 eV at 80 K; the solid line presents the calculated RIXS spectra of incident X-ray energy 707.5 eV.

the Fe^{2+}O_6 octahedra, which in turn couple to the neighbouring Fe^{3+}O_6 octahedra constituting the trimerons, although, as mentioned earlier, they are Jahn-Teller-inactive in the first approximation. Our results are consistent with the locally distorted structure of the FeO_6 octahedra and the short-range order above T_V observed by X-ray absorption⁴⁸ and diffuse scattering²⁹. These short-range correlations are polaronic in nature^{23,26,27,29,49}. Because a local molecular field and a tetragonal Jahn-Teller polaronic distortion are required to correctly simulate the excitation energy, the observed spin-orbital excitations are, indeed, magnetic polarons.

The magnitude of obtained $\Delta_{t_{2g}}$ is comparable with the $3d$ spin-orbit coupling strength, and thus confirms the observation of the unquenched orbital moment⁵⁰, which is known from work on Fe^{2+} impurities in MgO thin films⁵¹. These results are also consistent with conclusions of band-structure calculations using the monoclinic $P2/c$ crystal structure of magnetite⁹ (see Supplementary Note 3 and Supplementary Fig. 7), which give an energy splitting ~ 50 meV between minority-spin d_{xy} and d_{yz}/d_{zx} bands at the Γ point, conforming to the deduced $\Delta_{t_{2g}}$.

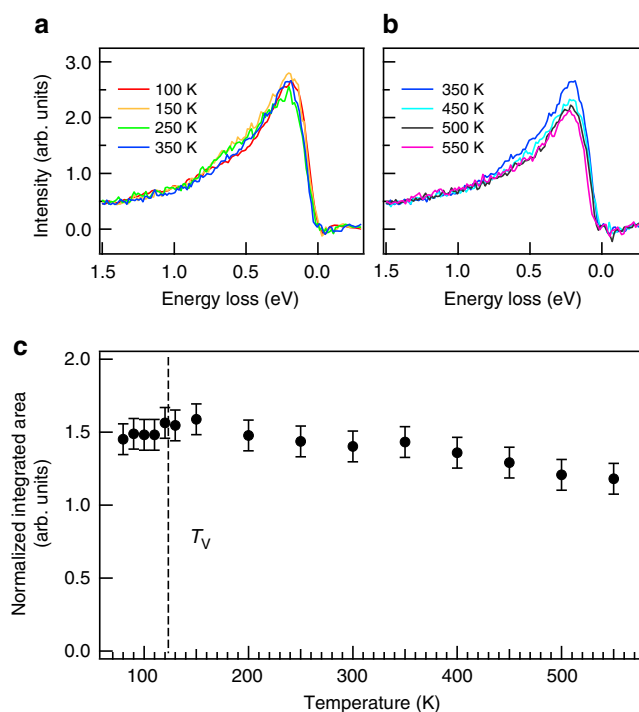


Figure 4 | Temperature-dependent spin-orbital excitations of Fe_3O_4 .

(a,b) RIXS spectra after the subtraction of the elastic component at selected temperatures. The spectra were recorded with the incident X-ray energy set to 706 eV. (c) Plot of the integrated 200-meV RIXS intensity versus temperature. The data were analysed by subtracting the elastic component from the measured spectrum and normalizing to the intensity of the dd excitation feature at 2.8 eV (see Supplementary Fig. 9). The dashed line indicates the Verwey transition temperature T_V . The RIXS data comprise an average of four runs of experimental results. The error bars are deduced from the average value of variations in the spectral intensity of four sets of measurements.

We also performed RIXS measurements above the Verwey transition and found that the spin-orbital excitations driven by polaronic distortion do exist in the cubic phase of Fe_3O_4 at high temperatures as shown in Fig. 2e and Supplementary Fig. 8. Figure 4 plots the temperature-dependent RIXS spectra with the incident X-ray energy set to the pre-edge absorption at 706 eV, an incident X-ray energy at which the elastic component is weak and the RIXS arises predominantly from octahedral Fe^{2+} ions with a negligible contribution from Fe^{3+} . The temperature-dependent results show that, when the temperature is varied across T_V , the spin-orbital excitation of 200 meV does not abruptly change its intensity and persists at least up to 550 K, albeit with a gradual decrease above 350 K. We interpret this as a gradual weakening of the polarons. RIXS results shown here serve as a fast probe to snapshot the dynamic lattice-spin-orbital excitations of Fe_3O_4 . These temperature-dependent RIXS results indicate that the FeO_6 octahedra are already locally distorted in the cubic phase of magnetite, in good agreement with the existence of the short-range correlations in the lattice structure above T_V . The temperature dependence of these distortions follows that of the magnetization of magnetite, suggesting short-range ordering of the Jahn-Teller distortion, which gets weakened as the temperature approaches the Curie temperature T_C , and providing further evidence for magnetic polarons. These observations suggest that the local distortion in the cubic phase could be attributed to the precursor of the monoclinic phase across the Verwey transition.

To summarize, our results demonstrate the usefulness of RIXS to unravel the local electronic structure of a mixed-valence compound by selecting the energy and polarization of incident X-rays. We revealed *dd* excitons in magnetite that have an energy centroid 200 meV and arise from polaronic distortion-driven spin-orbital excitations, which are best explained as magnetic polarons. We also applied crystal-field multiplet calculations to obtain the t_{2g} crystal field $\Delta_{t_{2g}} = -26 \pm 4$ meV induced by the tetragonal Jahn-Teller distortion. These results are consistent with the mechanism of ordering trimers for the Verwey transition. It would be interesting to carry out RIXS experiments with an improved energy resolution to study the change of spin-orbital excitations across the Verwey transition.

Methods

RIXS measurements. Using the AGM-AGS spectrometer at beamline 05A1 of the Taiwan Light Source³¹, we measured RIXS on a single-crystal $\text{Fe}_3\text{O}_4(001)$ at incident photon energies set to specific energies about the $L_3(2p_{3/2} \rightarrow 3d)$ absorption edge of Fe. See Supplementary Fig. 2a for the scattering geometry. Both the scattering angle ϕ defined as the angle between the incident and the scattered X-rays, and the incident angle θ from the crystal *ab* plane, were variable. The polarization of the incident X-ray was switchable between π and σ polarizations, that is, the polarization within and perpendicular to the scattering plane, respectively, and the polarization of scattered X-rays was not analysed. The energy bandwidth of the incident X-rays was 500 meV, and the total RIXS energy resolution was ~ 80 meV because the energy compensation method was used to ensure a high-resolution measurement in the energy-loss scheme³¹. The beam diameter of incident X-ray at the sample is ~ 0.5 mm.

Sample preparation. Single-crystal growth of magnetite was carried out in an infrared image furnace in high-purity argon gas (99.999% purity) atmosphere. Measurements of the temperature-dependent specific heat and resistivity of the synthesized magnetite crystal showed that it exhibits a sharp first-order Verwey transition at $T_V = 122$ K. The synthesized single crystal has a chemical composition of $\text{Fe}_{3(1-\delta)}\text{O}_4$ with $|\delta| \leq 0.00018$, indicative of a nearly ideal chemical stoichiometry. See Supplementary Figs 10 and 11 for the sample characterization.

Multiplet calculations. We undertook crystal-field multiplet RIXS calculations of *B*-site Fe^{2+} and Fe^{3+} using CTM4RIXS⁵² and MISSING (Dallera and Gusmeroli <http://www.esrf.eu/computing/scientific/MISSING/>) with the scattering angle 90° and the magnetization axis perpendicular to the scattering plane or in the scattering plane with angles 20° or 70° to the incident beam. The polarization of incident X-rays was selected to be π -polarized. Since the polarization of scattered X-rays was not analysed in the measurements, we summed calculated RIXS spectra of scattered X-rays with σ and π polarizations. We used a Lorentzian broadening 0.2 eV for the lifetime width of the intermediate states. The calculated spectra are obtained as an average of the spectra calculated for magnetic domains with the easy axis along the [100], [010] and [001] directions. The crystal-field parameter $10Dq$ was set to 1.13 eV, and the Slater integrals were reduced to 79% of their atomic values for accurately reproducing the *dd* excitation energies.

Data availability. The data that support the findings of this study are available from the corresponding authors on request.

References

- Bragg, W. H. The structure of magnetite and the spinels. *Nature* **95**, 561–561 (1915).
- Verwey, E. J. W. Electronic conduction of magnetite and its transition point at low temperatures. *Nature* **144**, 327–328 (1939).
- Walz, F. The Verwey transition—a topical review. *J. Phys. Condens. Matter* **14**, R285–R340 (2002).
- De Jong, S. *et al.* Speed limit of the insulator-metal transition in magnetite. *Nat. Mater.* **12**, 882–886 (2013).
- Almeida, T. P. *et al.* Visualized effect of oxidation on magnetic recording fidelity in pseudo-single-domain magnetite particles. *Nat. Commun.* **5**, 5154 (2014).
- Veintemillas-Verdaguer, S. *et al.* Magnetic nanocrystals for biomedical applications. *Prog. Cryst. Growth Charact. Mater.* **60**, 80–86 (2014).
- Wright, J. P., Attfield, J. P. & Radaelli, P. G. Long range charge ordering in magnetite below the Verwey transition. *Phys. Rev. Lett.* **87**, 266401 (2001).
- Wright, J. P., Attfield, J. P. & Radaelli, P. G. Charge ordered structure of magnetite below the Verwey transition. *Phys. Rev. B* **66**, 214422 (2002).
- Jeng, H.-T., Guo, G. Y. & Huang, D. J. Charge-orbital ordering and Verwey transition in magnetite. *Phys. Rev. Lett.* **93**, 156403 (2004).
- Leonov, I., Yaresko, A. N., Antonov, V. N., Korotin, M. A. & Anisimov, V. I. Charge and orbital order in Fe_3O_4 . *Phys. Rev. Lett.* **93**, 146404 (2004).
- Jeng, H. T., Guo, G. Y. & Huang, D. J. Charge-orbital ordering in low-temperature structures of magnetite: GGA + U investigations. *Phys. Rev. B* **74**, 195115 (2006).
- Huang, D. J. *et al.* Charge-orbital ordering and Verwey transition in magnetite measured by resonant soft X-ray scattering. *Phys. Rev. Lett.* **96**, 096401 (2006).
- Nazarenko, E. *et al.* Resonant X-ray diffraction studies on the charge ordering in magnetite. *Phys. Rev. Lett.* **97**, 056403 (2006).
- Schlappa, J. *et al.* Direct observation of t_{2g} orbital ordering in magnetite. *Phys. Rev. Lett.* **100**, 026406 (2008).
- Senn, M. S., Wright, J. P. & Attfield, J. P. Charge order and three-site distortions in the Verwey structure of magnetite. *Nature* **481**, 173–176 (2012).
- Senn, M. S., Loa, I., Wright, J. P. & Attfield, J. P. Electronic orders in the Verwey structure of magnetite. *Phys. Rev. B* **85**, 125119 (2012).
- Senn, M. S., Wright, J. P., Cumby, J. & Attfield, J. P. Charge localization in the Verwey structure of magnetite. *Phys. Rev. B* **92**, 024104 (2015).
- Ihle, D. & Lorenz, B. Small-polaron band versus hopping conduction in Fe_3O_4 . *J. Phys. C* **18**, L647–L650 (1985).
- García, J. *et al.* Resonant ‘forbidden’ reflections in magnetite. *Phys. Rev. Lett.* **85**, 578–581 (2000).
- Subías, G. *et al.* Magnetite, a model system for mixed-valence oxides, does not show charge ordering. *Phys. Rev. Lett.* **93**, 156408 (2004).
- Piekarz, P., Parlinski, K. & Oleś, A. M. Mechanism of the Verwey transition in magnetite. *Phys. Rev. Lett.* **97**, 156402 (2006).
- Hoesch, M. *et al.* Anharmonicity due to electron-phonon coupling in magnetite. *Phys. Rev. Lett.* **110**, 207204 (2013).
- Park, S. K., Ishikawa, T. & Tokura, Y. Charge-gap formation upon the Verwey transition in Fe_3O_4 . *Phys. Rev. B* **58**, 3717–3720 (1998).
- Chainani, A., Yokoya, T., Morimoto, T., Takahashi, T. & Todo, S. High-resolution photoemission spectroscopy of the Verwey transition in Fe_3O_4 . *Phys. Rev. B* **51**, 17976–17979 (1995).
- Park, J. H., Tjeng, L. H., Allen, J. W., Metcalf, P. & Chen, C. T. Single-particle gap above the Verwey transition in Fe_3O_4 . *Phys. Rev. B* **55**, 12813–12817 (1997).
- Schrupp, D. *et al.* High-energy photoemission on Fe_3O_4 : small polaron physics and the Verwey transition. *Europhys. Lett.* **70**, 789–795 (2005).
- Taguchi, M. *et al.* Temperature dependence of magnetically active charge excitations in magnetite across the Verwey transition. *Phys. Rev. Lett.* **115**, 256405 (2015).
- Anderson, P. W. Ordering and antiferromagnetism in ferrites. *Phys. Rev.* **102**, 1008–1013 (1956).
- Bosak, A. *et al.* Short-range correlations in magnetite above the Verwey temperature. *Phys. Rev. X* **4**, 011040 (2014).
- Ament, L. J. P., van Veenendaal, M., Devereaux, T. P., Hill, J. P. & van den Brink, J. Resonant inelastic x-ray scattering studies of elementary excitations. *Rev. Mod. Phys.* **83**, 705–767 (2011).
- Lai, C. H. *et al.* Highly efficient beamline and spectrometer for inelastic soft X-ray scattering at high resolution. *J. Synchrotron Radiat.* **21**, 325–332 (2014).
- Kuiper, P., Searle, B. G., Duda, L. C., Wolf, R. M. & Van der Zaag, P. J. Fe $L_{2,3}$ linear and circular magnetic dichroism of Fe_3O_4 . *J. Electron. Spectrosc. Relat. Phenom.* **86**, 107–113 (1997).
- Chen, J. *et al.* Magnetic circular dichroism in Fe $2p$ resonant photoemission of magnetite. *Phys. Rev. B* **69**, 085107 (2004).
- Arenholz, E., van der Laan, G., Chopdekar, R. V. & Suzuki, Y. Anisotropic X-ray magnetic dichroism at the Fe $L_{2,3}$ edges in Fe_3O_4 . *Phys. Rev. B* **74**, 094407 (2006).
- Braicovich, L. *et al.* Magnetic excitations and phase separation in the underdoped $\text{La}_{2-x}\text{Sr}_x\text{CuO}_4$ superconductor measured by resonant inelastic X-ray scattering. *Phys. Rev. Lett.* **104**, 077002 (2010).
- Zhou, K. J. *et al.* Persistent high-energy spin excitations in iron-pnictide superconductors. *Nat. Commun.* **4**, 1470 (2013).
- Huang, H. Y. *et al.* Raman and fluorescence characteristics of resonant inelastic X-ray scattering from doped superconducting cuprates. *Sci. Rep.* **6**, 19657 (2016).
- de Groot, F. M. F., Kuiper, P. & Sawatzky, G. A. Local spin-flip spectral distribution obtained by resonant x-ray Raman scattering. *Phys. Rev. B* **57**, 14584–14587 (1998).
- van Veenendaal, M. Polarization dependence of L- and M-edge resonant inelastic X-ray scattering in transition-metal compounds. *Phys. Rev. Lett.* **96**, 117404 (2006).
- Jia, C. J. *et al.* Persistent spin excitations in doped antiferromagnets revealed by resonant inelastic light scattering. *Nat. Commun.* **5**, 3314 (2014).
- Haverkort, M. W. Theory of resonant inelastic X-ray scattering by collective magnetic excitations. *Phys. Rev. Lett.* **105**, 167404 (2010).
- Bisogni, V. *et al.* Bimagnon studies in cuprates with resonant inelastic X-ray scattering at the O *K* edge. I. Assessment on La_2CuO_4 and comparison with the excitation at Cu L_3 and Cu *K* edges. *Phys. Rev. B* **85**, 214527 (2012).

43. Lee, W. S. *et al.* Role of lattice coupling in establishing electronic and magnetic properties in quasi-one-dimensional cuprates. *Phys. Rev. Lett.* **110**, 265502 (2013).
44. Gasparov, L. V. *et al.* Infrared and Raman studies of the Verwey transition in magnetite. *Phys. Rev. B* **62**, 7939–7944 (2000).
45. Gasparov, L. V. *et al.* Magnetite: Raman study of the high-pressure and low-temperature effects. *J. Appl. Phys.* **97**, 10A922 (2005).
46. McQueeney, R. J. *et al.* Investigation of the presence of charge order in magnetite by measurement of the spin wave spectrum. *Phys. Rev. B* **73**, 174409 (2006).
47. McQueeney, R. J. *et al.* Zener double exchange from local valence fluctuations in magnetite. *Phys. Rev. Lett.* **99**, 246401 (2007).
48. Subías, G., García, J. & Blasco, J. EXAFS spectroscopic analysis of the Verwey transition in Fe₃O₄. *Phys. Rev. B* **71**, 155103 (2005).
49. Ihle, D. & Lorenz, B. Small-polaron conduction and short-range order in Fe₃O₄. *J. Phys. C* **19**, 5239–5251 (1986).
50. Huang, D. J. *et al.* Spin and orbital magnetic moments of Fe₃O₄. *Phys. Rev. Lett.* **93**, 077204 (2004).
51. Haupricht, T. *et al.* Local electronic structure of Fe²⁺ impurities in MgO thin films: temperature-dependent soft X-ray absorption spectroscopy study. *Phys. Rev. B* **82**, 035120 (2010).
52. Stavitski, E. & de Groot, F. M. F. The CTM4XAS program for EELS and XAS spectral shape analysis of transition metal L edges. *Micron* **41**, 687–694 (2010).

Acknowledgements

We thank A. Fujimori, J. Paul Attfield, Jeroen van de Brink, Sumio Ishihara, Chun-Fu Chang, Maurits Haverkort and Hebatalla Elnaggar for valuable discussions. We acknowledge Martin Beye for sharing unpublished results with us. This work was supported in part by the Ministry of Science and Technology of Taiwan under Grant No. 103-2112-M-213-008-MY3. J.-S.Z. was supported by the DOD-ARMY grant (W911NF-16-1-0559) in USA. J.-G.P. was supported by the research programme of the Institute for Basic Science (IBS-R009-G1) in Korea.

Author contributions

All authors made significant contributions. H.Y.H., Z.Y.C., W.B.W., J.O. and A.S. performed RIXS measurements. H.Y.H., R.-P.W. and F.M.F.d.G. performed multiplet

calculations. H.-T.J. and G.Y.G. performed band-structure calculations. C.T.C. designed the RIXS beamline and spectrometer. Z.-Y.L. and J.-S.Z. synthesized and prepared the magnetite single crystals. D.J.H., H.Y.H., F.M.F.d.G., A.C., J.-S.Z., J.-G.P. and L.H.T. analysed the data, discussed the results and wrote the paper. D.J.H. is responsible for project planning.

Additional information

Supplementary Information accompanies this paper at <http://www.nature.com/naturecommunications>

Competing interests: The authors declare no competing financial interests.

Reprints and permission information is available online at <http://npg.nature.com/reprintsandpermissions/>

How to cite this article: Huang, H. Y. *et al.* Jahn-Teller distortion driven magnetic polarons in magnetite. *Nat. Commun.* **8**, 15929 doi: 10.1038/ncomms15929 (2017).

Publisher's note: Springer Nature remains neutral with regard to jurisdictional claims in published maps and institutional affiliations.



Open Access This article is licensed under a Creative Commons Attribution 4.0 International License, which permits use, sharing, adaptation, distribution and reproduction in any medium or format, as long as you give appropriate credit to the original author(s) and the source, provide a link to the Creative Commons license, and indicate if changes were made. The images or other third party material in this article are included in the article's Creative Commons license, unless indicated otherwise in a credit line to the material. If material is not included in the article's Creative Commons license and your intended use is not permitted by statutory regulation or exceeds the permitted use, you will need to obtain permission directly from the copyright holder. To view a copy of this license, visit <http://creativecommons.org/licenses/by/4.0/>

© The Author(s) 2017